Nano Research

Open Access

Research Article

Robust, biomimetic, superhydrophobic coating with flame-retardant properties and excellent self-extinguishing performance

Mingxuan Zhang[1,§], Yuechang Lian[1,§ ✉], Haonan Liu[1,§], Siyuan Xiang[2], Yutao Wang[1], Bo Yang[1], Shengyang Tao[1 ✉], Michael Kappl[3], and Wendong Liu[1 ✉]

[1] *Dalian Key Laboratory of Intelligent Chemistry, School of Chemistry, Dalian University of Technology, Dalian 116024, China*
[2] *Academy of Food Interdisciplinary Science, School of Food Science and Technology, Dalian Polytechnic University, Dalian 116034, China*
[3] *Department of Physics at Interfaces, Max Planck Institute for Polymer Research, Ackermannweg 10, D-55128 Mainz, Germany*
[§] *Mingxuan Zhang, Yuechang Lian, and Haonan Liu contributed equally to this work.*

Cite this article: *Nano Research*, **2026**, *19*, 94908394. https://doi.org/10.26599/NR.2026.94908394

ABSTRACT: Flame-retardant coatings are crucial for safety. However, flame-retardant materials are often hydrophilic, causing them to easily dissolve in high-humidity environments, thereby significantly limiting their durability. Thus, the integration of water repellency and flame retardancy into a single coating is ideal for developing durable and flame-retardant materials. In this study, a robust skin-inspired double-layer coating was fabricated by using spray coating. An intumescent flame-retardant "dermis" layer, comprising ammonium polyphosphate (APP), polydopamine (PDA), and 1-[3-(trimethoxysilyl) propyl]urea (UPTMS), provides the primary heat insulation and flame retardancy functions. A superhydrophobic "epidermis" layer, constructed using silicone nanofilaments (Si NFs), poly(vinylidene fluoride-co-hexafluoropropylene) (PVDF-HFP), and triethoxy-1H,1H,2H,2H-heptadecafluorodecylsilane (PFDTS), protects flame-retardant materials in moist conditions. Owing to its intumescent effect, the obtained coating demonstrated excellent flame retardancy, with the fire self-extinguishing immediately after the removal of flame source. It achieves a limiting oxygen index (LOI) of 85.3% and significantly decreases the peak heat release rate (PHRR) and the fire growth index (FGI) of 59.20 $kW \cdot m^{-2}$ and 0.789 $kW \cdot m^{-2} \cdot s^{-1}$, respectively. The epidermal layer demonstrated outstanding superhydrophobicity and remarkable mechanical stability, with the water contact angle remaining above 160° after 1000 bending cycles between 90° and 180°. Together with the facile spray-coating process, the biomimetic design of this intumescent flame-retardant and superhydrophobic coating provides a feasible and sustainable strategy for constructing durable fireproofing materials.

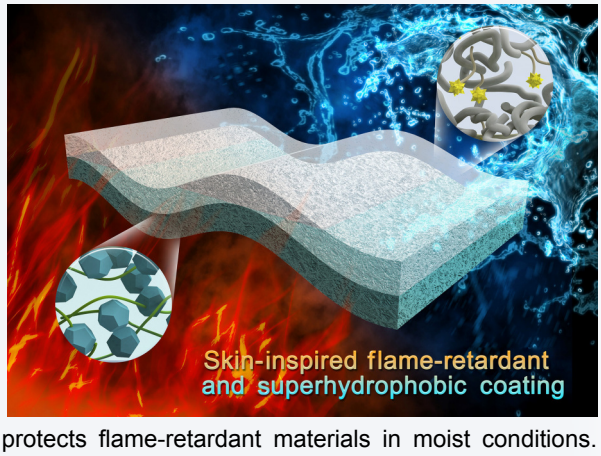

KEYWORDS: coating, flame-retardant, superhydrophobic, spray coating, biomimetic

1 Introduction

Combustible materials such as plastics, textiles, and building materials are highly flammable and easily ignited, triggering severe fire hazards. Each year, fires and the hazardous substances released during combustion result in more than tens of thousands of deaths and substantial property damage [1, 2]. Therefore, enhancing the flame retardancy of combustible materials is crucial for broadening their applications and safeguarding human lives [3, 4]. Flame-retardant (FR) modification methods generally fall into two categories: integrating flame-retardant additives into the bulk combustible materials or constructing a flame-retardant coating on the surface [5]. However, the former often alters the inherent properties of the pristine materials and is limited by the maximum doping quantity, resulting in insignificant flame retardancy [6]. In comparison, surface coatings are more commonly used because their processing methods and coating features can be tailored to meet specific application requirements. Although they are still acceptable, flame-retardant coatings are more hydrophilic and

Received: October 15, 2025; **Revised:** December 10, 2025
Accepted: December 31, 2025

✉Address correspondence to Wendong Liu, liuwendong@dlut.edu.cn; Yuechang Lian, 13102968173@mail.dlut.edu.cn; Shengyang Tao, taosy@dlut.edu.cn

mechanically fragile; their performance declines when exposed to moisture for prolonged periods [7]. Therefore, developing coatings that combine flame retardancy and waterproofing properties is of great significance for fundamental research and practical applications.

In recent years, superhydrophobic materials have attracted significant attention [8, 9]. Since the successful fabrication of bionic lotus leaf structures, researchers have developed a variety of micro- and nanofabrication techniques to prepare materials with exceptional water repellency [10, 11]. The synergy between surface roughness and low surface energy causes water droplets to rest in a Cassie state on superhydrophobic surfaces, effectively preventing the liquid from wetting the substrate and demonstrating waterproof functionality [12]. Thus, superhydrophobic materials offer significant potential for self-cleaning [13], anti-corrosion [14, 15], anti-icing [16, 17], drag reduction [18, 19], and other applications, thereby providing new opportunities to explore the cross-dimensional integration of natural hydrophobic mechanisms and flame-retardant properties.

Superhydrophobicity can be integrated with flame-retardant materials in a specific manner [20–22]. The most versatile approach involves blending hydrophobic materials with flame retardants, where the hydrophobic components provide liquid repellency and act as binders to enhance the adhesion of the flame retardants [23–25]. Long et al. used a low-surface-energy polydimethylsiloxane (PDMS) binder with a curing agent to adhere $ZnSn(OH)_6$ particles to a substrate. After solidification, a flame-retardant superhydrophobic coating was obtained. It achieved a water contact angle (CA) of 158° and a water sliding angle (SA) of 1°, with a limiting oxygen index (LOI) value of 44% [24]. Liu et al. fabricated the flame-retardant superhydrophobic cotton by immersing it in an ammonium polyphosphate (APP)-based flame-retardant solution followed by spraying it with an epoxy resin binder. The modified cotton extinguished the flame within 20 s in a vertical combustion experiment and exhibited a water CA of 162° [25]. However, many hydrophobic components used as adhesives are inherently combustible, thereby compromising the flame retardancy of coatings [26]. Therefore, constructing robust, flame-retardant, and waterproofed layered composite coatings is a practical alternative approach. Taking advantage of the electrostatic interactions and chemical bonding between molecules, Shi et al. engineered a flame-retardant coating by combining phosphorylated poly(ethyleneimine) with hydrophobically modified ammonium polyphosphate via a layer-by-layer self-assembly technique. The resulting coated cotton fabrics exhibited excellent flame retardancy [27]. Jiang et al. developed a composite flame-retardant superhydrophobic coating via a combined coating and deposition approach, using aluminium hydroxide, APP, PDMS, and candle soot as raw materials. The CA reached 154° and withstood ignition for 14 s under continuous flame exposure [28]. Similarly, Zhang et al. prepared a flame-retardant superhydrophobic coating composed of APP, sodium montmorillonite, and vinyltrimethoxysilane using the self-assembly technique and sol-gel reaction. The coating demonstrated a maximum heat release rate (HRR) of 19.37 $W \cdot g^{-1}$ [29]. Despite these achievements, challenges persist in preparing flame-retardant superhydrophobic materials, including high costs, complex fabrication processes, reliance on specialized equipment (e.g., vapor deposition, electrospinning, and layer-by-layer self-assembly), and limited scalability [30, 31]. Therefore, developing robust, flame-retardant, and superhydrophobic materials via a facile and low-cost fabrication process is essential.

Learning from nature is one of the most critical strategies for the design and fabrication of functional materials. Owing to the uniquely designed double-layer structure, human skin has a good barrier protection function. The epidermis is a dense waterproof barrier that can effectively prevent water loss and foreign liquid invasion and protect the structural stability of the inner layer, and the dermis is composed of rich fibers and cells, with good mechanical strength, and it can perform physiological functions such as thermal insulation [32]. The double-layered structure of human skin provides a natural example of how layered structures achieve functional integration, offering a new pathway to improve the stability and performance of flame-retardant coatings under complex environmental conditions by mimicking this natural structure. Herein, we propose a skin-inspired intumescent flame-retardant and superhydrophobic coating with excellent self-extinguishing properties and robustness. The APP- and 1-[3-(trimethoxysilyl)propyl]urea (UPTMS)-dominated intumescent flame-retardant layer mimics the dermal layer to provide heat insulation and flame retardancy. Meanwhile, a superhydrophobic layer composed of silicone nanofilaments, poly(vinylidene fluoride-co-hexafluoropropylene) (PVDF-HFP), and triethoxy-1H,1H,2H,2H-heptadecafluorodecylsilane (PFDTS) mimics the epidermis layer protecting the flame-retardant materials from moisture. The obtained coating demonstrated excellent flame retardancy, self-extinguishing fire immediately after the flame source was removed, and a limiting oxygen index (LOI) of 85.3% was achieved. The epidermal layer exhibited outstanding water repellency across a wide pH range (CA > 156° and SA < 14° at pH 1–13). Moreover, the biomimetic coating exhibits remarkable mechanical stability and durability, with the water contact angle remaining above 160° after 1000 bending cycles between 90° and 180°, thereby endowing the biomimetic coating durable flame retardancy in harsh environments. The key innovation in our design lies in decoupling the distinctive requirements of waterproofing and flame-retardancy into two layers, while ensuring the stability and continuity of the double-layered coatings. Together with the facile spray-coating process, the biomimetic design of this intumescent flame-retardant and superhydrophobic coating offers a feasible, cost-efficient, and sustainable strategy for constructing durable fireproofing materials, with potential applications in construction materials, pipe insulation, energy storage, and interior plastics.

2 Results and discussion

2.1 Preparation of skin-inspired flame-retardant and superhydrophobic coatings

Inspired by the bilayer architecture of human skin, which comprises a dense epidermal surface and an inner dermal layer, we fabricated an intumescent flame-retardant and superhydrophobic coating (Fig. 1(a) and Fig. S1 in the Electronic Supplementary Material (ESM)). The outer "epidermal" layer, PVDF-HFP, functions similarly to keratinocytes by stabilizing its components, including silicone nanofilaments, to form a protective barrier that prevents the infiltration of liquid or solid impurities. The inner "dermal" layer is mainly formulated with APP and UPTMS. Similar to the functional components in the dermis (e.g., collagen and blood vessels), the continuous and stable coating formed by UPTMS condensation provides structural support and thermal insulation. Meanwhile, APP can prevent flame damage by

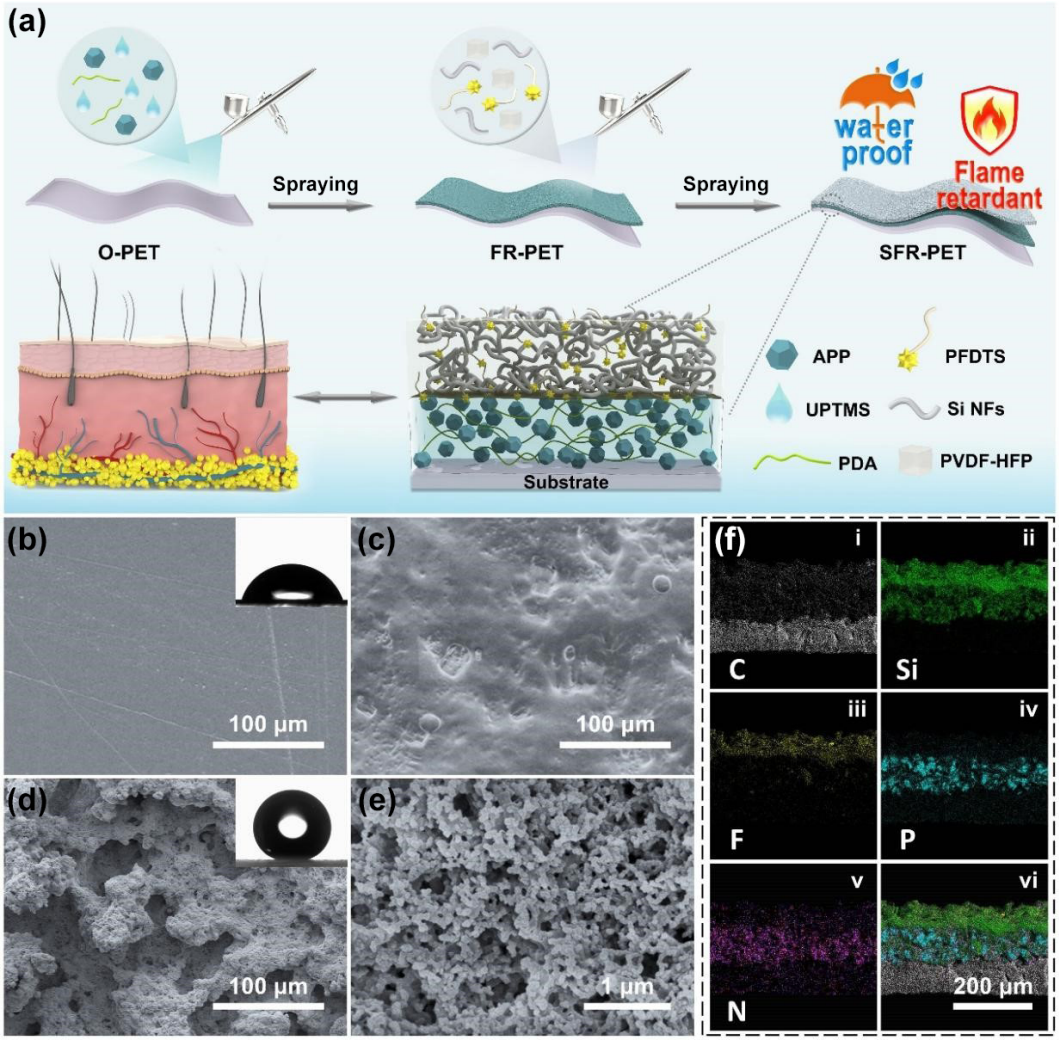

Figure 1 Preparation of skin-inspired flame-retardant and superhydrophobic coating. (a) Schematic illustration of skin-inspired flame-retardant superhydrophobic coating fabrication by stepwise spraying. SEM images of (b) O-PET, (c) FR-PET, and ((d) and (e)) SFR-PET. (f) C, Si, F, P, and N elemental mapping of the cross-section of the double-layered SFR-PET.

absorbing heat and releasing non-flammable gases during thermal degradation. This bionic structure ensures both environmental stability and functional durability.

Pristine polyethylene terephthalate (O-PET) has a flat and smooth surface and demonstrates the hydrophilicity, with a water CA of about 72° (Fig. 1(b) and Fig. S2(a) in the ESM). Subsequently, a flame-retardant stock solution containing APP, UPTMS, and polydopamine (PDA) was sprayed onto the O-PET to obtain a flame-retardant layer (FR-PET). The amount of the stock solution for spraying was set to 0.3 mL·cm^{-2} to form a relatively uniform film that thoroughly covered the O-PET substrate. As shown in Fig. 1(c) and Fig. S2(b) in the ESM, the synergy between UPTMS and PDA ensured that the micrometer-sized APP particles were completely wrapped without forming isolated loose aggregates. The strong electrostatic interaction between the negatively charged APP particles and positively charged UPTMS promoted cohesive dispersion [20, 33]. PDA formed by the self-polymerization of dopamine (DA) improved the adhesion between the components. The distributions of P and N elements in the FR layer further confirmed the homogeneity and continuity (Fig. S3(a) in the ESM). To protect the FR layer from water damage, a superhydrophobic layer was prepared by spraying a mixture of silicone nanofilaments (Si NFs), PVDF-HFP, and PFDTS onto the FR-PET. During the deposition of silicone nanofilaments, the confinement effect caused by solvent evaporation leads to the formation of porous and microscale protrusions. Although PVDF-HFP and PFDTS were interspersed between the Si NFs, they functioned as cohesive agents, binding the constituent Si NFs together and providing the necessary low surface energy. This configuration trapped air beneath water droplets, yielding a Cassie state with the CA reaching 165° (Figs. 1(d) and 1(e), and Fig. S2(c) in the ESM). The scanning electron microscopy (SEM) images in Fig. 1 confirm that the skin-inspired flame-retardant and superhydrophobic coating (SFR-PET) was successfully fabricated via spray coating.

A skin-inspired double-layer coating was visible in the cross section of the SFR-PET (Fig. S2(d) in the ESM). The bottom flame-retardant layer is ~ 77.9 μm thick, comprising APP particles well embedded within the continuous UPTMS. It mimicked the dermis and connected to the polymer substrate (Fig. S3(b) in the ESM). The porous top layer, approximately 65.3 μm thick, mimicked the epidermis and maintained water droplets in the Cassie state,

thereby providing waterproof functionality (Fig. S2(c) in the ESM). This double-layered coating successfully integrated liquid repellency and flame retardancy, providing a practical enhancement for durable flame-retardant materials. Moreover, the elemental mapping of C, Si, F, P, and N obtained via energy dispersive X-ray spectroscopy (EDS) analysis of the cross-section of the SFR-PET further verified the successful fabrication of the skin-inspired coating (Fig. 1(f)).

The chemical components and functional groups of the PET substrate before and after coating were characterized using Fourier transform infrared (FTIR) spectroscopy and X-ray photoelectron spectroscopy (XPS). The attenuated total reflection-FTIR (ATR-FTIR) spectra of the pristine polyester (PET) film (Figs. 2(a) and 2(b)) showed characteristic peaks at 1713, 2968, and 3430 cm^{-1}, corresponding to the symmetrical stretching vibration of C=O, C–H, and O–H, respectively [34]. After flame-retardant deposition, the characteristic peak at 3319 cm^{-1} corresponded to the N–H stretching vibration in APP and UPTMS [35, 36]. The firm absorption peaks at 872 and 1243 cm^{-1} are attributed to the asymmetric stretching vibration of P–O–P and the symmetric stretching vibration of P=O in APP, respectively [37], indicating the successful introduction of inflammable APP. The peaks around 1015 and 1713 cm^{-1} indicated the asymmetric stretching vibration of Si–O–Si and the stretching vibration of the C=O bonds, respectively, confirming the hydrolysis and condensation of UPTMS [20]. In addition, the absorption peak at 1437 cm^{-1} originated from C–N in UPTMS and PDA [37], while the peak between 1500 and 1600 cm^{-1} corresponded to C=C in the aromatic ring of PDA, proving the integration of APP, UPTMS, and PDA into the FR-PET. For the SFR-PET, the peak at 1269 cm^{-1} belonged to the C–F bonds in PFDTS and PVDF-HFP [38], whereas the peak near 1015 cm^{-1} corresponded to the Si–O–Si bond in the Si NFs. The additional enhancement at 780 cm^{-1} was attributed to the stretching vibration of the Si–C bond in the PFDTS and Si NFs [35]. Moreover, FR-PET and SFR-PET had weaker absorption peaks in the range of 600–1400 cm^{-1} than O-PET. This is because the flame-retardant and superhydrophobic layers had specific thicknesses that masked the substrate's absorption peaks of the substrate, showing only their own absorption peaks. The elemental compositions of the coated samples were further evaluated by XPS analysis (Fig. 2(c)). Compared to the O-PET, which mainly contains C and O, FR-PET exhibited the characteristic peaks of N 1s, Si 2p, and P 2p, accompanied by a decrease in the C 1s signal, which was attributed to the deposition of APP, UPTMS, and PDA. High-resolution spectra revealed energy peaks at 134.3, 285.7, and 399.4 eV, corresponding to P–O, C–N/C–Si, and –NH_2 bonds,

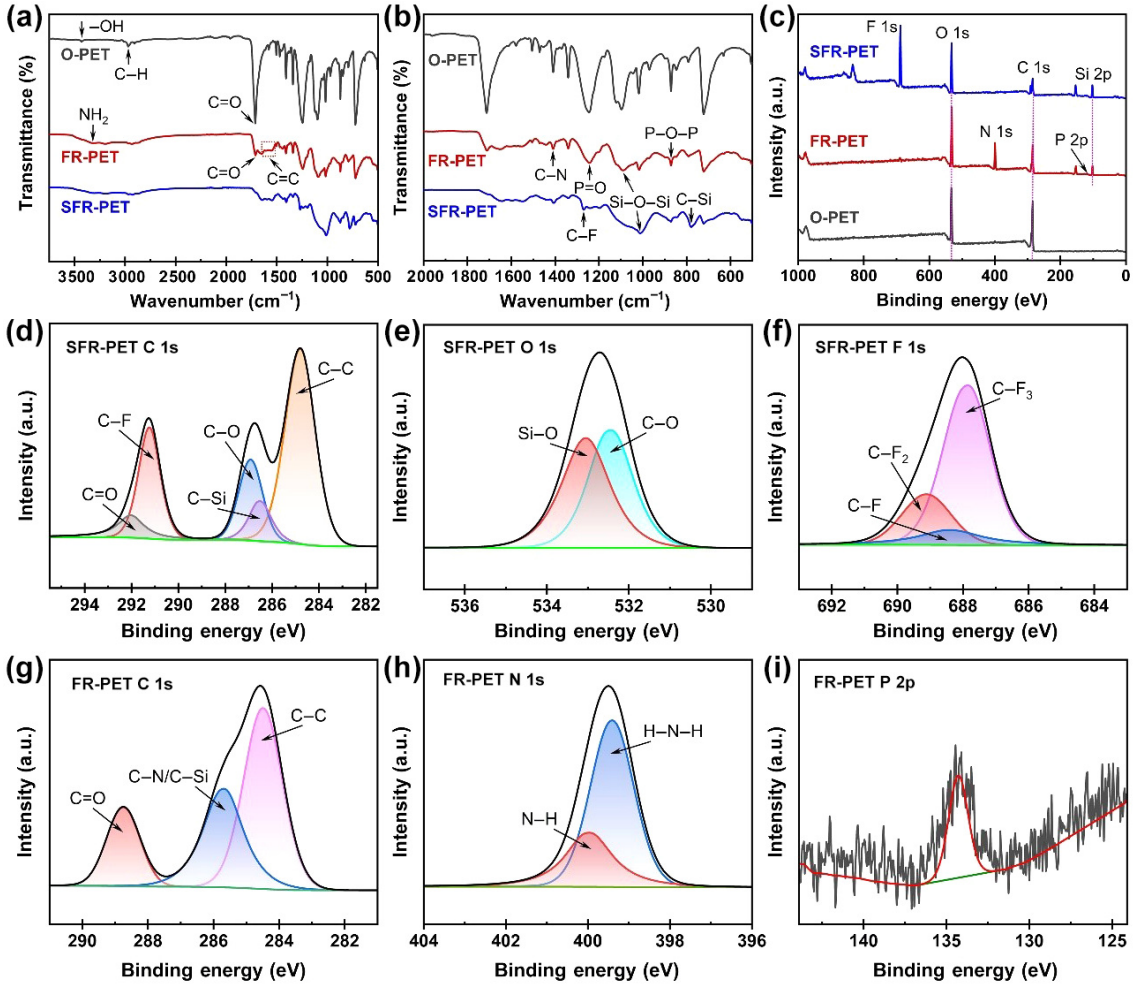

Figure 2 Composition characteristics of the PET substrate before and after spray coating. (a) and (b) ATR-FTIR spectra of O-PET, FR-PET, and SFR-PET. (c) XPS spectra of O-PET, FR-PET, and SFR-PET. High-resolution XPS spectra for (d) C 1s, (e) O 1s, and (f) F 1s of SFR-PET. High-resolution XPS spectra for (g) C 1s, (h) N 1s, and (i) P 2p of FR-PET.

respectively (Figs. 2(g)–2(i)). Another feature peak of F 1s was observed for the SFR-PET, accompanied by a further decrease in the C 1s and O 1s signals, which was attributed to the coverage of the Si NFs, PVDF-HFP, and PFDTS. The energy peaks at 284.8, 286.6, 532.5, 533.1, 689.1, and 688.4 eV corresponded to C–C, C–Si, C–O, Si–O, F–C–F, and C–F bonds, respectively (Figs. 2(d)–2(f)). These results validate the successful integration of flame-retardant and superhydrophobic materials into the skin-inspired coatings to achieve excellent flame retardancy and robustness.

2.2 Wettability and robustness of the biomimetic coating

The deposition of Si NFs and PVDF-HFP provided the coating with the necessary roughness and low surface energy, thus endowing it with superhydrophobicity, which is essential for achieving long-term durability. Upon water immersion, the coating exhibited the characteristic "silver mirror" effect, indicating the presence of an air layer and Cassie wetting (Fig. S4(a) in the ESM). The liquid repellency can be further optimized by introducing PFDTS to reduce the surface tension. As shown in Fig. S4(b) in the ESM, the apparent contact angle of SFR-PET increased with the dosage of PFDTS. The highest contact angle of 165° was achieved at a PFDTS dosage of 15 μL, indicating outstanding superhydrophobicity (Fig. S4(b) in the ESM). However, a further increase in the amount of PFDTS decreased the apparent contact angle, owing to the formation of a slippery-like surface. The optimized liquid repellency ensured that the biomimetic coating exhibited low adhesion and self-cleaning behaviors. Its low surface adhesion was evident from the ease with which water droplets could be removed under deformation. Even under compression, the deformed droplets detached without tailing or splitting (Fig. 3(a)). This property was further evidenced by the rolling off (Movie S1 in the ESM) and dragging (Movie S2 in the ESM) of water droplets on inclined (tilt angle around 4°) and horizontally placed SFR-PET, respectively. The self-cleaning performance of the SFR-PET was evaluated by contaminating the surface with sand (Fig. 3(b)). The continuous deposition of water droplets thoroughly washed the sand away, keeping the film clean and dry. This good self-cleaning performance highlights the ability of biomimetic coating to resist contamination in practical applications.

In addition to pure water, the as-prepared coating also effectively repelled various liquid mixtures commonly encountered in daily life. Tea, milk, coffee, cola, and milk tea droplets maintained a spherical morphology without spreading (Fig. 3(c)), with contact angles above 160° and sliding angles below 10° in aqueous solutions (Fig. 3(d)). Emulsions, such as milk and coffee, showed sliding angles below 15° (Fig. 3(d)). The coating also exhibited excellent resistance across a broad pH range (1–13), with the highest contact angles around 165° and sliding angles below 6°, ensuring its suitability in harsh environments (Fig. 3(e)). The contact angle increased to a peak and then gradually decreased within this pH range. This is attributed to the fact that the high electronegativity of the F atoms in PVDF-HFP can alter the surface charge of the superhydrophobic layer. Therefore, an electric double layer formed between the solid and liquid surfaces. Under acidic or alkaline conditions, when the ion concentrations are high, the thickness of the double layer decreases, and the screening effect increases, thereby reducing the surface tension at the liquid–solid interface and thus the contact angle [39, 40]. Additionally, the Si–OH groups in the superhydrophobic layer can be protonated or deprotonated, which contributes to the reduction in contact angle [41].

The biomimetic design ensured that the coating is mechanically robust (Fig. S5 in the ESM). As shown in Fig. 3(f) and Fig. S6 in the ESM, after 1000 bending cycles between 90° and 180°, no significant change in the surface microstructure was observed, and the contact angle remained above 160° on both sides of the SFR-PET. The biomimetic coating also exhibited durable repellence against water flow in the bent state. This robustness stems from the synergistic effects of the interactions within and between the

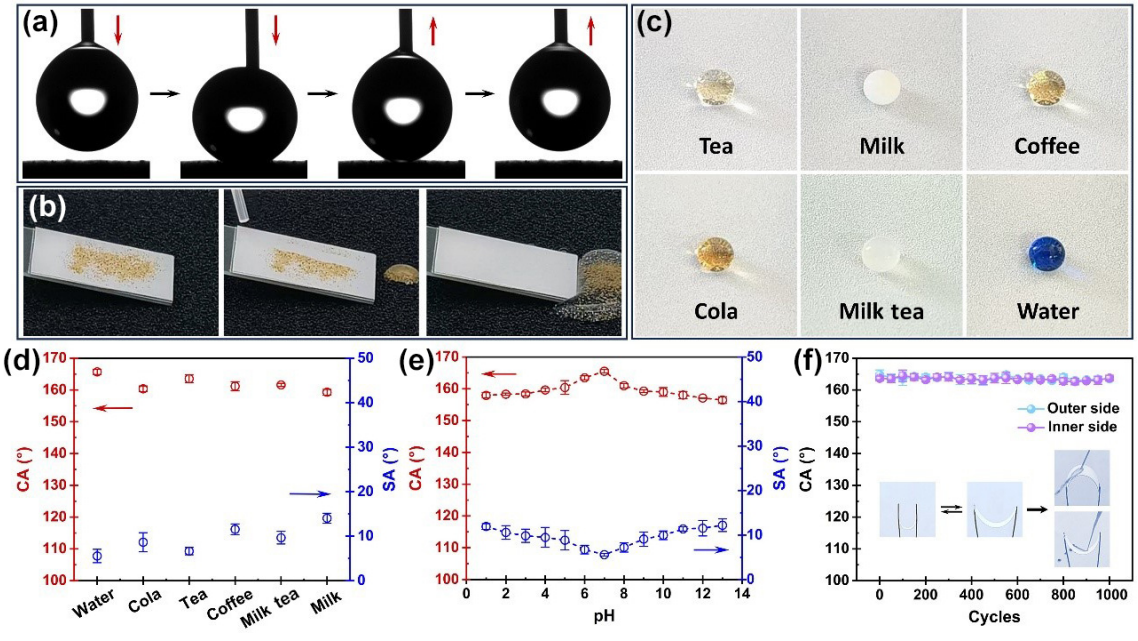

Figure 3 Liquid repellency and mechanical stability of SFR-PET. (a) Adhesion behaviour of a water droplet on SFR-PET. (b) Images of the self-cleaning process of SFR-PET. (c) Images of 20 μL of tea, milk, coffee, cola, milk tea, and water (stained with methylene blue) droplets deposited on SFR-PET. (d) CA and SA of probe liquids on SFR-PET. (e) CA and SA of droplets with different pH values. (f) CA of the SFR-PET after repeated bending cycles. The insets show that the SFR-PET is bent at angles from 90° to 180°, and the coating maintains stable superhydrophobicity to flowing water after 1000 bending cycles.

coating layers. In the flame-retardant layer, the strong electrostatic interactions between the negatively charged APP particles and positively charged UPTMS promote the formation of a continuous and stable structure [20, 33]. Simultaneously, PDA, formed by the self-polymerization of DA, enhances the adhesion between the flame retardants and the PET substrate. For the superhydrophobic layer, the PVDF-HFP and PFDTS interspersed between the Si NFs serve as cohesive agents, binding the constituent Si NFs together and thereby imparting the layer with flexibility and mechanical robustness. The interfacial interactions between the two functional layers also contribute to the structural integrity. The fluorine atoms in the PVDF-HFP have relatively strong electronegativity and form hydrogen bonds with the amino groups of UPTMS and APP in the flame-retardant layer [42]. The PFDTS, located at the interface between the two layers, can establish hydrophobic–hydrophobic interactions with the PVDF-HFP through its perfluoroalkyl group. Meanwhile, it forms covalent Si–O–Si bonds with the UPTMS in the underlying layer via the hydrolysis and condensation of the two silanes, thereby imparting a robust connection between the functional layers. In addition, UPTMS forms covalent Si–O–C bonds with the substrate and the hydrogen bonds between PDA and the PET substrate. The synergistic effect of these multiscale interactions ensures the robustness of the biomimetic coating, making it highly promising for long-term practical applications.

2.3 Exceptional flame retardancy

A thermogravimetry-differential scanning calorimetry (TG-DSC) analysis was conducted under nitrogen and air atmospheres to evaluate the thermal decomposition behaviour of the PET substrates before and after coating. We first modulated the ratio of UPTMS to APP to guide the optimization of the flame-retardant layer composition (Fig. S7 in the ESM). As shown in Figs. 4(a)–4(c) and Table 1, the 5% weight loss temperature ($T_{5\%}$) of O-PET was 386.0 °C, and the char residue at 800.0 °C was only 12.3%. However, $T_{5\%}$ of FR-PET was 127.7 °C, and the char residue increased to 38.7%, mainly due to the promotion effect of phosphoric and polyphosphoric acids generated by APP during the formation of the char layer and the inorganic SiO_2 generated by UPTMS, which contributed to the increase in residue weight [43]. Furthermore, FR-PET exhibited a new and broader endothermic peak at 333.0 °C in the DSC test. $T_{5\%}$ of SFR-PET was 202.3 °C, and the char residue increased to 46.6 wt.%. The presence of silica materials generated from the degradation of Si NFs and PFDTS in the superhydrophobic layer further thickened the protective barrier and enhanced the thermal resistance [23].

In the meantime, polymer components in the superhydrophobic layer caused a sharper endothermic peak to shift to 307.5 °C [44]. These results showed that the polymer substrate was effectively protected during high-temperature degradation under the synergistic action of the flame-retardant and the superhydrophobic coating (Fig. S8 in the ESM). Derivative thermogravimetry (DTG) further demonstrated the flame-retardancy of the coating. As shown in Fig. 4(b), SFR-PET exhibited a reduced maximum mass loss rate of 0.23 wt.%·°C^{-1}, which was significantly lower than those

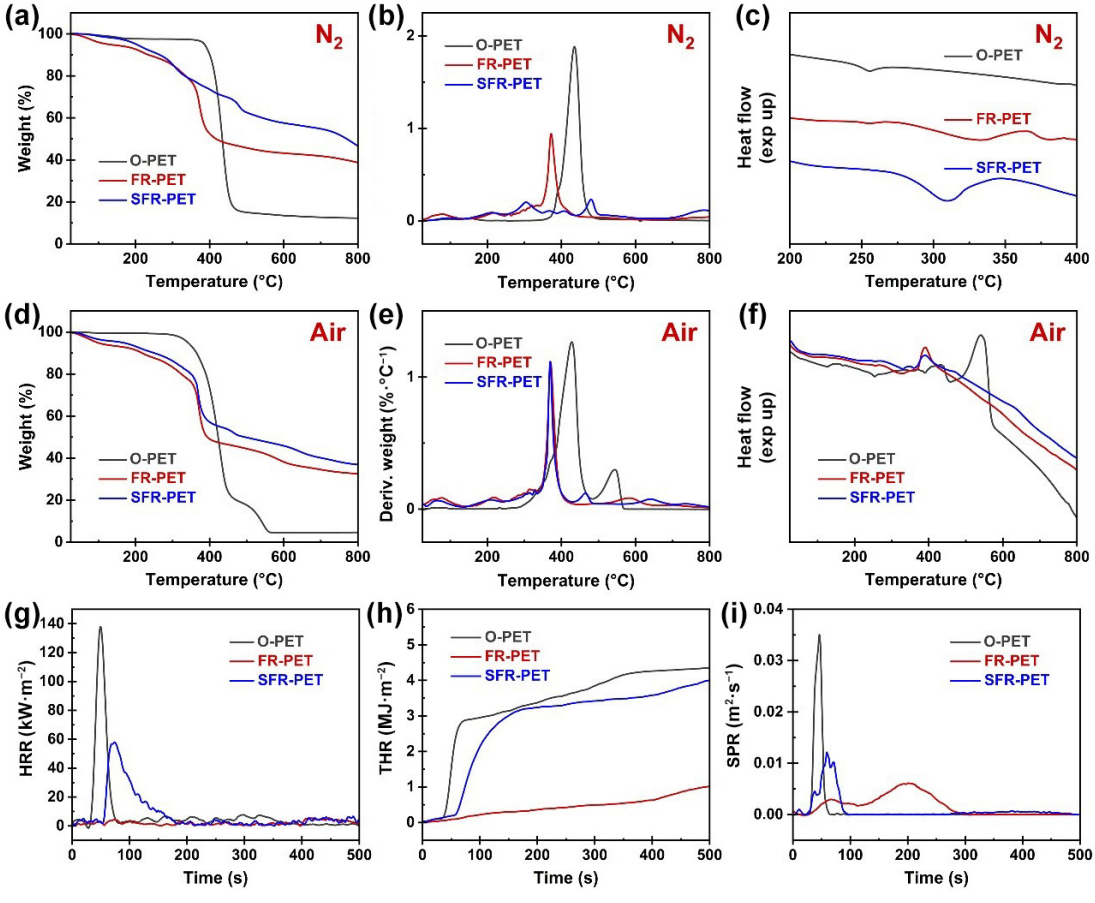

Figure 4 Fire retardancy. ((a) and (d)) TG, ((b) and (e)) DTG, and ((c) and (f)) DSC curves of O-PET, FR-PET, and SFR-PET in ((a)–(c)) N_2 and ((d)–(f)) air. (g) HRR, (h) THR, and (i) SPR curves of O-PET, FR-PET, and SFR-PET.

Table 1 Thermogravimetric analysis data of the coated and uncoated materials under nitrogen and air atmospheres

Gas	Sample	$T_{5\%}$ (°C)	T_{1max} (°C)	T_{2max} (°C)	R_{max} (wt.%·°C^{-1})	Residue at 800 °C (wt.%)
N_2	O-PET	386.0	434.8	—	1.88	12.3
	FR-PET	127.7	372.3	—	0.94	38.7
	SFR-PET	202.3	304.1	480.1	0.23	46.6
Air	O-PET	341.4	427.7	544.1	1.27	4.6
	FR-PET	97.2	370.6	582.2	1.11	32.6
	SFR-PET	164.9	369.4	464.7	1.12	36.9

of FR-PET and O-PET by 0.94 wt.%·°C^{-1} and 1.88 wt.%·°C^{-1}, respectively, demonstrating the improved thermal stability and flame retardancy imparted by the biomimetic coating.

TG results for the air atmosphere are shown in Fig. 4(d) and Table 1. Because of the presence of oxygen, the decomposition rates of FR-PET and SFR-PET increased markedly; however, the biomimetic coating still exhibited excellent protective effects on the material. The results showed that $T_{5\%}$ of O-PET is 341.4 °C and the char residue is only 4.6 wt.% at 800.0 °C. Compared to FR-PET and SFR-PET, the coating demonstrated protective effects similar to those observed under a nitrogen atmosphere. Based on the DTG and DSC curves (Figs. 4(e) and 4(f)), R_{max} of FR-PET and SFR-PET increases due to the oxidative degradation of polymers contained in the substrate and superhydrophobic layer [35]. However, it remained 0.15 wt.%·°C^{-1} lower than that of O-PET. Meanwhile, the endothermic peak transformed into an exothermic peak of varying intensity. However, the heat release of SFR-PET was lower than those of O-PET and FR-PET, indicating that the biomimetic coating inhibited thermal oxidative degradation. The combustion behavior of SFR-PET was further evaluated using cone calorimetric measurements, which are powerful for investigating flame-retardant materials under realistic fire scenarios. Some essential parameters, including the heat release rate (HRR), total heat release (THR), smoke production rate (SPR), total smoke production (TSP), CO production rate (COP), and CO_2 production rate (CO_2P), were recorded as functions of time. The critical combustion data are summarized in Figs. 4(g)–4(i) and Table 2, and Fig. S9 in the ESM.

O-PET exhibited high flammability and released a large amount of heat, with a peak HRR (PHRR) of 145.83 kW·m^{-2} and a THR of 4.35 MJ·m^{-2}. The corresponding values of FR-PET were 7.11 kW·m^{-2} and 1.01 MJ·m^{-2}, which were significantly reduced by 95.1% and 76.8%, respectively, indicating the excellent flame retardancy of the flame-retardant coating. Although SFR-PET did not exhibit the lowest PHRR, it still showed a 59.4% reduction compared to O-PET, and its THR value reached 4.01 MJ·m^{-2} at 500 s. We attribute the enhancement of the PHRR and THR of the SFR-PET to the presence of the polymer (PVDF-HFP) in the superhydrophobic layer, which contributed to additional heat release upon decomposition. The coating also influenced the smoke production. The release of CO and CO_2 from O-PET reached the highest level at approximately 60 s, with release rates of 0.003 and 0.083 g·s^{-1}, respectively. In contrast, the highest release rates of CO and CO_2 from FR-PET were reduced by 45.6% and 73.5%, respectively. Similarly, the release rates of those gases decreased by approximately 50.0% for SFR-PET (Figs. S9(b) and S9(c) in the ESM). Notably, although FR-PET showed a higher TSP than O-PET (Fig. S9(a) in the ESM), owing to the generation of non-combustible agglomerates derived from the thermal decomposition of the flame-retardant layer, SFR-PET exhibited the lowest TSP, which was attributed to the suppression of smoke release from the inner layer by the superhydrophobic layer. These results highlight the synergistic contribution of the flame-retardant and superhydrophobic layers, which caused the excellent flame retardancy and self-extinguishing properties of the biomimetic coating (Fig. S10 in the ESM).

Table 2 Comparison of flame retardancy performances of O-PET, FR-PET, and SFR-PET

	O-PET	FR-PET	SFR-PET
PHRR (kW·m^{-2})	145.83	7.11	59.20
TPHRR (s)	49	415	75
THR (MJ·m^{-2})	4.35	1.01	4.01
PSPR (m^2·s^{-1})	0.036	0.0087	0.014
TSP (m^2)	0.54	0.81	0.48
TTI (s)	31	—	55
LOI (%)	21.44	81.45	85.30
FPI (s·m^2·kW^{-1})	0.21	—	0.93
FGI (kW·m^{-2}·s^{-1})	2.976	0.017	0.789
TRP (s$^{1/2}$·kW·m^{-2})	194.9	—	259.6
PSEA[a] (m^2·kg^{-1})	1040.5324	775.3466	806.0830

[a]Peak specific extinction area (PSEA); a parameter to measure and monitor the amount of smoke arising from combustion.

The fire performance index (FPI) and fire growth index (FGI) are two widely used parameters to evaluate the flame retardancy of a material [45, 46]. Generally, the higher the FPI and the lower the FGI, the higher the flame retardancy of the material. As demonstrated in Eq. (1), FPI was derived from the proportion of ignition time (t_{ign}) to PHRR, while FGI (Eq. (2)) was derived from the proportion PHRR to the time to PHRR (t_{PHRR}), respectively [4]. O-PET exhibited a low FPI of 0.21 s·m^2·kW^{-1} and a high FGI of 2.976 kW·m^{-2}·s^{-1}, suggesting its high flammability (Table 2). In comparison, the biomimetic SFR-PET showed a significantly higher FPI of 0.93 s·m^2·kW^{-1} and a lower FGI of 0.789 kW·m^{-2}·s^{-1}, indicating excellent flame retardancy. The thermal response parameter (TRP) reflects ignition time delay when a material is exposed to an external thermal flux. A higher TRP reflects a longer ignition time. According to Eq. (3), the TRP of O-PET is 194.9 s$^{1/2}$·kW·m^{-2}, given that the polymer substrate is highly flammable; thus, the 35 kW·m^{-2} is much higher than the critical heat flux value. In comparison, the TRP of the SFR-PET is 259.6 s$^{1/2}$·kW·m^{-2}, confirming that the coating is more difficult to ignite.

$$\mathrm{FPI} = t_{ign}/\mathrm{PHRR} \quad (1)$$

$$\mathrm{FGI} = \mathrm{PHRR}/t_{\mathrm{PHRR}} \quad (2)$$

$$\mathrm{TRP} = q_{\mathrm{ex}}\sqrt{t_{\mathrm{ign}}} \quad (3)$$

Vertical flame combustion tests were conducted on O-PET, FR-PET, and SFR-PET, using a butane gas burner to ignite the samples (Figs. 5(a)–5(c) and Movies S3–S5 in the ESM). The O-PET ignited instantly upon contact with the pilot flame, and the flame spread quickly along the sample, becoming bright and vigorous (Movie S3 in the ESM). The pristine PET burned out within 3 s and was accompanied by a large amount of black smoke.

In contrast, no obvious flame was observed when the FR-PET was in contact with the pilot flame. After 10 s of ignition, it had only a 2.5 cm charred black surface, accompanied by black smoke, and the flame self-extinguished immediately upon removal of the pilot flame (Movie S4 in the ESM). The SFR-PET exhibited the combustion behavior similar to that of FR-PET, but it had a shorter scorched black area (2.0 cm), indicating better flame retardancy (Movie S5 in the ESM). The LOI tests were also conducted to assess the flame retardancy of the as-prepared coating. As shown in Fig. S11 in the ESM, O-PET exhibited an LOI of only 21.44%. FR-PET and SFR-PET reached LOIs of 81.45% and 85.3%, respectively, which are nearly four times that of the uncoated substrate, indicating that FR-PET and SFR-PET exhibit strong flame retardancy.

In addition to the flame retardancy, the biomimetic coating exhibited excellent thermal insulation (Fig. 5(d) and Fig. S12 in the ESM). Upon heating, a silica-rich layer was formed on SFR-PET, effectively reducing heat transfer. In the temperature range of 70–170 °C, SFR-PET and FR-PET lowered surface temperatures by an average of 40.59% and 30.30%, respectively, compared to O-PET (Fig. 5(e)). In addition, the surface heating test was conducted by depositing O-PET, FR-PET, and SFR-PET on a hot plate at 100 °C (Fig. 5(f)). Notably, the O-PET used here has a thickness of ~ 500 μm, which is significantly thicker than FR-PET

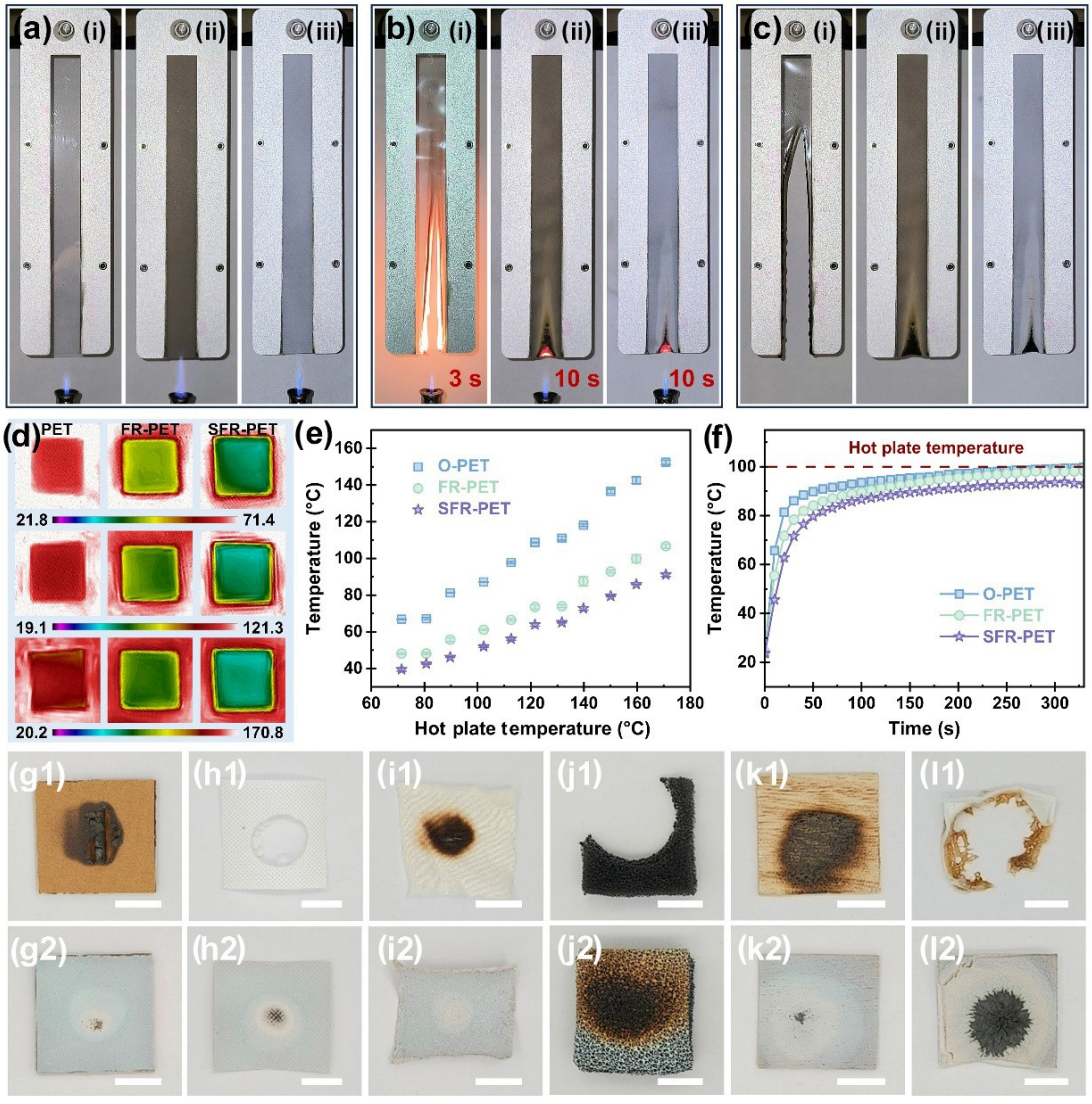

Figure 5 Flame combustion tests and thermal conductivity. Optical images obtained in vertical flame combustion test of (i) O-PET, (ii) FR-PET, and (iii) SFR-PET at the status of (a) the original, (b) during the ignition, and (c) after the igniter removed. (d) Infrared imaging and (e) variation of the surface temperature of O-PET, FR-PET, and SFR-PET after 10 s of heating on a hot plate. (f) Variation curve of the surface temperature of O-PET (500 μm), FR-PET, and SFR-PET after being deposited on a hot plate at 100 °C. Optical images of (g) the flammable cardboard, (h) nonwoven PP fabric, (i) cotton textile, (j) polyurethane sponge, (k) plywood, and (l) PS foam without (1) and with (2) superhydrophobic flame-retardant coating after ignition, the scale bars represent 2 ((g)–(i)) and 1 cm ((j)–(l)), respectively.

or SFR-PET, thereby eliminating the impact of thickness on thermal insulation performance. The SFR-PET temperature increased more slowly than that of O-PET. Its surface temperature was 6.7 °C lower than that of O-PET at 330 s (Fig. 5(f)), indicating that the flame-retardant superhydrophobic coating had strong thermal insulation.

The fabrication approach presented here is primarily based on spray coating, which offers the flexibility to fabricate superhydrophobic flame-retardant coatings on various flammable substances. As shown in Fig. S13 in the ESM, the biomimetic coating exhibits strong adhesion, particularly on hydrophilic and/or high-surface-roughness materials such as O-PET, plywood, and cotton textiles. Uncoated materials, such as flammable cardboard, nonwoven PP fabric, cotton textile, polyurethane sponge, plywood, and PS foam, were severely damaged upon ignition (Figs. 5(g1)–5(l1)). In contrast, the same materials coated with the skin-inspired flame-retardant and superhydrophobic coating retained their original morphologies (Figs. S14 and S15 in the ESM). Even for the highly flammable substrates such as nonwoven PP fabric, polyurethane sponge, and PS foam, the coating effectively prevented perforation and significant burn damage (Figs. 5(g2)–5(l2)). These results confirmed that the flame-retardant superhydrophobic coating can be broadly applied to enhance the safety and durability of a wide range of materials in practical settings.

2.4 Flame-retardant mechanism

The flame-retardant behavior of the SFR-PET was preliminarily predicted and studied through structural and chemical analyses after combustion. SEM images from different regions (upper, middle, and lower positions as demonstrated by the dashed boxes) of SFR-PET after vertical combustion (Fig. 6(a)) revealed spatial differences in the microstructure. The middle region retained a relatively dense superhydrophobic layer compared with the porous upper region (Figs. 6(b1), 6(b2), 6(c1), and 6(c2)). By contrast, a porous but continuous carbonaceous layer developed in the lower region (Figs. 6(d1) and 6(d2)), indicating that a protective char barrier was formed during combustion. These observations suggest that the flame retardancy of SFR-PET stems from its inner intumescent effect, in which the coating expands and chars upon heating. The resulting char layer acted as a physical barrier to heat and oxygen, whereas the release of flame-retardant gases contributed to the self-extinguishing of the flame.

To further understand the thermal degradation process, a thermogravimetric (TG)-FTIR analysis was conducted to investigate the gaseous products released during pyrolysis. The three-dimensional (3D) TG-FTIR patterns (Figs. 6(e) and 6(f)) and corresponding FTIR spectra (Figs. 6(g) and 6(h)) were obtained for both the flame-retardant and superhydrophobic layers at different temperatures. For the flame-retardant layer, no significant pyrolysis

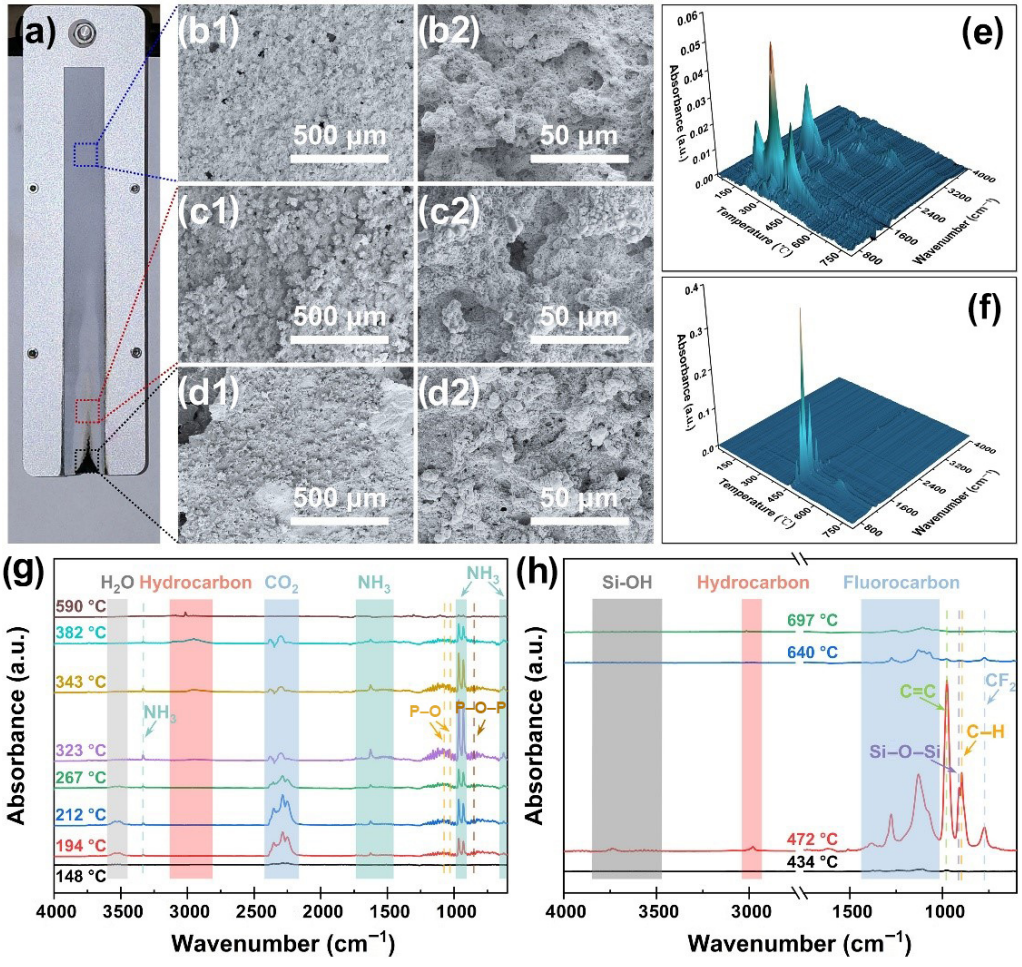

Figure 6 Flame-retardant mechanism. (a) Photographs of SFR-PET after the vertical flame burning test. (b1)–(d2) SEM images of SFR-PET at different positions after vertical combustion. ((e) and (f)) 3D TG-FTIR patterns and ((g) and (h)) the corresponding FTIR maps of pyrolyzed volatiles of ((e) and (g)) flame-retardant layer and ((f) and (h)) superhydrophobic layer at different temperatures.

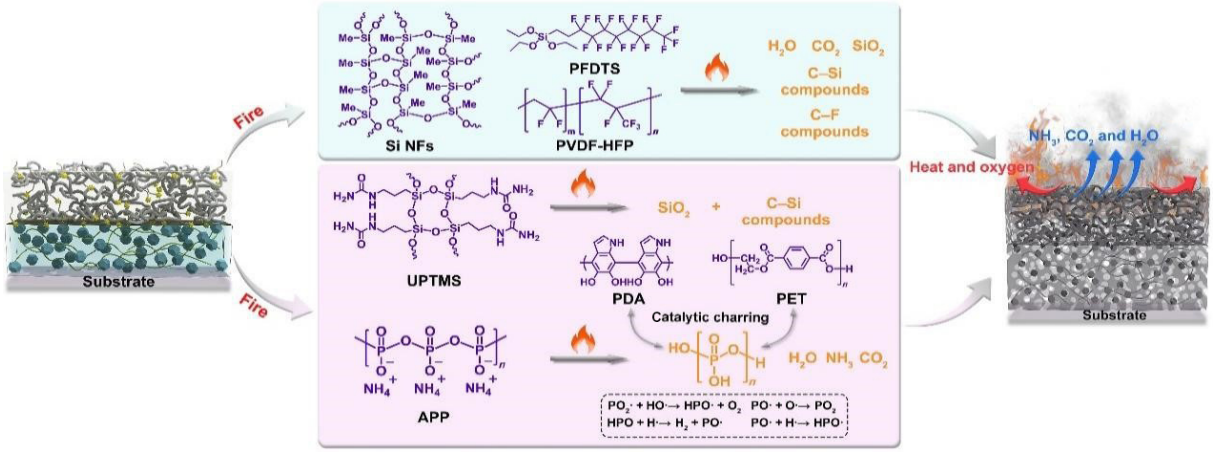

Figure 7 Scheme of the flame-retardant mechanism of the skin-inspired coating.

products were detected below 148 °C. At this temperature, the first adsorption peak was observed around 2300 cm^{-1}, corresponding to CO_2 production [47, 48]. Additional peaks emerged simultaneously at 194 °C, indicating the release of NH_3, with characteristic peaks at 628, 930, 964, 1626, and 3300 cm^{-1} (Figs. S16(a) and S16(b) in the ESM) [49, 50]. Hydrocarbon-related bands near 3000 cm^{-1} also appeared [23], alongside a broad band at 3500 cm^{-1} attributable to water generated by dehydration reaction between the acid generated by the decomposition of APP and the hydroxyl group in the coating [23, 35]. In addition, trace amounts of phosphoric acid, polyphosphoric acid, and PO· radicals were also be produced upon heating APP, as suggested by the fingerprint peaks near 930 and 964 cm^{-1} (Fig. 6(g)) [23]. In the superhydrophobic layer, thermal degradation at around 472 °C yielded Si–O–Si (911 cm^{-1}) and C–H (897 cm^{-1}) species, indicating the breakdown of silicone nanofilaments [23, 51]. The cleavage of low-energy C–C bonds in PVDF-HFP leads to the formation of fluorocarbon fragments, as evidenced by characteristic peaks for C=C (977 cm^{-1}), CF (1078 and 1130 cm^{-1}), CF_2 (774 and 1277 cm^{-1}), and CF_3 (1385 cm^{-1}) fluorocarbon compounds resulting from the cleavage of low-energy C–C bonds (Fig. 6(h), and Fig. S16(c) and S16(d) in the ESM) [52–56].

Based on the above test results, a possible flame-retardancy mechanism was proposed (Fig. 7). The superhydrophobic layer releases thermally stable silicon- and fluorine-containing compounds that form a physical barrier to heat and oxygen. Simultaneously, the flame-retardant layer emits large quantities of NH_3, H_2O, and CO_2 during decomposition. These gases dilute the combustible volatiles and reduce the ambient oxygen concentration, creating an effective gas-phase barrier. The porous char structure formed during this process also slows the diffusion of the combustion products, effectively reducing smoke release. Furthermore, phosphoric and polyphosphoric acids formed during APP decomposition catalyze the carbonization of the underlying polymer and substrate, producing a robust char layer. This carbonaceous residue synergizes with the silica layer generated by the superhydrophobic components to form a thermally stable, fireproof, and heat-insulating barrier. The catalytic carbonization process also produces H_2O, reinforcing the gas-phase flame-retardant action. Additionally, PO· and related free radicals generated by the further decomposition of phosphoric acid capture reactive species such as O·, H·, and other reactive free radicals, interrupting free-radical chain reactions that sustain combustion. Overall, SFR-PET achieves flame retardancy through a combination of gas-phase dilution, solid-phase barrier formation, and free-radical quenching. This multi-level defense significantly slows the spread of flames and smoke release, resulting in impressive flame retardancy.

3 Conclusions

Inspired by the layered structure of human skin, we developed an intumescent flame-retardant and superhydrophobic coating using a facile and scalable spray-coating method. The design incorporated an outer superhydrophobic layer and an inner flame-retardant layer, which together delivered both water repellency and flame retardancy, resulting in a coating with excellent self-extinguishing and robust properties. The epidermal layer exhibited outstanding superhydrophobicity, with a static water CA of 165°, and retained its liquid repellency even after 1000 cycles of repeated bending between 90° and 180°. This mechanical durability highlights the potential of this coating for long-term use in flexible applications. Upon exposure to flame, the inner flame-retardant layer rapidly formed an intumescent char, while simultaneously releasing non-combustible gases. This combination effectively blocked heat and oxygen, causing the fire to self-extinguish immediately after the flame source is removed. The biomimetic coating achieved an LOI of 85.3% and significantly reduced the PHRR and FGI by 59.4% and 73.5%, respectively, compared to the pristine polymer substrate. Overall, this biomimetic, spray-applied intumescent flame-retardant and superhydrophobic coating is a promising strategy for fabricating robust and multifunctional flame-retardant materials. Its facile fabrication, combined with high thermal stability and mechanical robustness, offers substantial potential for scalable applications in safety-critical environments.

4 Experimental and method

4.1 Materials

APP ($n \geq 1000$), dopamine hydrochloride (DA-HCL, 98%), Tris (hydroxymethyl) aminomethane (Tris, biotech grade 99.9%), UPTMS (94%), and methyl trichlorosilane (TCMS, 99%) were supplied by Macklin. Toluene (≥ 99.5%), tetrahydrofuran (≥ 99.5%), and hydrochloric acid (HCl, AR 36%–38%) were

provided by Kermel. PVDF-HFP ($M_n \approx 130{,}000$) and rhodamine B (RhB, 95%) were purchased from Sigma-Aldrich. Absolute ethanol (AR) was provided by Tianjin Fuyu Fine Chemical Co., Ltd. PFDTS was received from TCI. PET films (100 and 500 μm thick) were ordered from Shenzhen Chifu Industry & Trade Co., Ltd., and cut into pieces for use as substrates. Si NFs were synthesized using a solution-based approach [57]. Deionized (DI) water with a resistivity of 18.25 MΩ·cm was produced using the Zhiang Clever-Q15UT water purification system. Different liquids used to characterize superhydrophobic properties (tea, milk, coffee, cola, and milk tea) were purchased from a local supermarket. The butane torch (Iroda PT-220) used for the vertical flame combustion test was provided by Pro-Iroda Industries, Inc.

4.2 Preparation of stock solutions

DA-HCL (0.04 g) and APP (1.75 g) were added to a Tris-HCl (20 mL) buffered aqueous solution, and the mixture was vortexed until a homogeneous dispersion was formed. Subsequently, UPTMS (2.5 g) was added to the dispersion. After treating the above mixture in an ultrasonic bath for 25 min, a dark-gray stock solution was obtained. For the fabrication of superhydrophobic coating, a homogeneous stock solution was formed by mixing a Si NF dispersion (6 mL, 0.0225 g·mL^{-1} in THF) and PVDF-HFP solution (3 mL, 0.03 g·mL^{-1} in THF) first, then PFDTS (15 μL) was added and the mixture was vortexed until a homogeneous phase was achieved.

4.3 Fabrication of skin-inspired flame-retardant superhydrophobic coatings

A flame-retardant and superhydrophobic coating was fabricated on a commercial polyester film by spray coating. O-PET films were first cleaned with toluene, acetone, and absolute ethanol under ultrasonic conditions and then dried under a nitrogen flow. A flame-retardant layer was first fabricated on the substrate by spraying the flame-retardant stock solution using a spray gun (nozzle diameter, 0.3 mm) at a vertical distance of ~ 25 cm with a spraying pressure of 60 psi. The sprayed stock solution was sprayed at 0.3 mL·cm^{-2} to obtain a uniform flame-retardant coating. Afterward, the coating was heated to completely evaporate the solvents, resulting in FR-PET. The superhydrophobic layer was prepared similarly, with the spraying distance regulated to ~ 15 cm and the amount of sprayed solution set to 0.4 mL·cm^{-2}. After this two-step spray-coating process, a film with flame retardancy and superhydrophobicity was obtained (SFR-PET). A skin-inspired intumescent flame-retardant superhydrophobic coating was fabricated on different substrates in the manner described above.

4.4 Characterization

The surface structure and elemental distribution of the films were characterized using SEM (NOVA NanoSEM 450, USA) equipped with EDS. The samples were sputter-coated with a 10 nm layer of Pt using a sputter coater (Q150T, UK) prior to avoiding charging. Static and sliding angles of 3 μL water droplets on the films were measured using a goniometer, Dataphysics OCA50 (Data Physics Instruments GmbH, Germany). The characteristics of the coated and uncoated films were analyzed using a Fourier transform infrared spectrometer under ATR (NICOLET iS50, USA). The elemental species and chemical bonding in the films were analyzed using XPS (Escalab Xi+, UK). Thermal insulation tests were conducted using an infrared thermal imager (FLIR ONE PRO, Teledyne FLIR, USA). Thermogravimetric and DSC analyses were performed using a simultaneous thermal analyzer (Q600, TA, USA) from 30 to 800 °C. The samples were analyzed under a nitrogen atmosphere with a heating rate of 10 °C·min^{-1}. Adhesion strength was measured by laito High Technology LT-M. TG-FTIR spectrometry was measured on a thermogravimetric instrument coupled with a Fourier transform infrared spectroscope (Netzsch STA449F5-Nicolet IS 20, manufacturer NETZSCH, Thermo Fisher, Germany). The TG-FTIR analysis was conducted in the temperature range of 40–800 °C under a nitrogen atmosphere, with heating rates and flow rates set to 10 °C·min^{-1} and 50 mL·min^{-1}, respectively.

Electronic Supplementary Material: Supplementary material (low adhesion, self-cleaning, mechanical stability, flame retardancy, thermal insulation performance, adhesion strength tests, and optimization of the ratio of UPTMS to APP in the flame-retardant layer; SEM images of O-PET, FR-PET, SFR-PET, original and coated raw materials after combustion, and the cross-section of the SFR-PET; the EDS analyses of the FR-PET and SFR-PET; optical images of silver mirror phenomenon of SFR-PET in water, the water CA of SFR-PET with different PFDTS contents, and FR-PET after combustion with different ratios of UPTMS and APP; the smoke production, and CO and CO_2 release of the O-PET, FR-PET, and SFR-PET; the TG, DTG, and heat flow of the coating with different ratios of UPTMS to APP; the LOI tests of the O-PET, FR-PET, and SFR-PET; schematic diagram of the thermal insulation test device; flammable substances with and without superhydrophobic flame-retardant coating after combustion; absorbance of representative pyrolysis volatiles from flame-retardant layer and superhydrophobic layer, as well as their TG/DTG curves (PDF). Videos demonstrate the low adhesion behavior of the superhydrophobic flame-retardant coating, as well as vertical flame combustion tests on O-PET, FR-PET, and SFR-PET (mp4)) is available in the online version of this article at https://doi.org/10.26599/NR.2026.94908394.

Data availability

All data needed to support the conclusions in the paper are presented in the manuscript and the Electronic Supplementary Material. Additional data related to this paper may be requested from the corresponding author upon request.

Acknowledgements

W. D. L. acknowledges the National Natural Science Foundation of China (NSFC) (No. 22205031), the Natural Science Foundation of Liaoning Province (Nos. 2025-MSLH-149 and 2022-MS-136), the Fundamental Research Funds for the Central Universities (No. DUT25Z2533), and the Open Project of State Key Laboratory of Supramolecular Structure and Materials (No. sklssm2023012) for financial support, and thanks Prof. Dr. Hans-Jürgen Butt for helpful discussions. S. Y. X. acknowledges the National Natural Science Foundation of China (NSFC) (No. 32401983) and the Major Scientific and Technological Cooperation Funds of Zhoushan (No. 2023C13012) for financial support. S. Y. T. acknowledges the National Natural Science Foundation of China (NSFC) (No. 22372025). The authors also acknowledge the assistance of DUT Instrumental Analysis Center.

Declaration of competing interest

All the contributing authors report no conflict of interest in this work.

Author contribution statement

M. X. Z.: Writing – original draft, conceptualization, investigation, methodology, formal analysis, data curation, writing – review & editing. Y. C. L.: Writing – review & editing, conceptualization, investigation, validation, data curation. H. N. L.: Writing – review & editing, formal analysis, investigation, validation, data curation. S. Y. X.: Data curation, visualization, funding acquisition, formal analysis. Y. T. W.: Writing – review & editing, investigation, validation. B. Y.: Writing – review & editing, investigation. S. Y. T.: Resources, writing – review & editing, funding acquisition. M. K.: Conceptualization, writing – review & editing, ssupervision. W. D. L.: Conceptualization, methodology, formal analysis, resources, data curation, writing – review & editing, supervision, funding acquisition. All the authors have approved the final manuscript.

Use of AI statement

None.

References

[1] Yeoh, G. H.; De Cachinho Cordeiro, I. M.; Wang, W.; Wang, C.; Yuen, A. C. Y.; Chen, T. B. Y.; Vargas, J. B.; Mao, G. Z.; Garbe, U.; Chua, H. T. Carbon-based flame retardants for polymers: A bottom-up review. *Adv. Mater.* **2024**, *36*, 2403835.

[2] Hou, B. Y.; Guo, Y.; Yang, Q. S.; Tang, L. C.; Shi, Y. Q.; Gao, J. F.; Pan, Y. T.; Hong, M.; Dinh, T.; Wang, H. et al. Mechanism-guided thermoelectric strategies for smart fire prevention. *Adv. Mater.* **2025**, *37*, 2508628.

[3] Ma, Z. W.; Feng, J. B.; Huo, S. Q.; Sun, Z. Q.; Bourbigot, S.; Wang, H.; Gao, J. F.; Tang, L. C.; Zheng, W.; Song, P. A. Mussel-inspired, self-healing, highly effective fully polymeric fire-retardant coatings enabled by group synergy. *Adv. Mater.* **2024**, *36*, 2410453.

[4] Panda, S.; Hajra, S.; Kim, H.; Seo, J.; Jeong, B.; Lee, I.; Kaja, K. R.; Belal, M. A.; Vivekananthan, V.; Khanbareh, H. et al. An overview of flame-retardant materials for triboelectric nanogenerators and future applications. *Adv. Mater.* **2025**, *37*, 2415099.

[5] Ma, Z. W.; Zhang, J. Z.; Maluk, C.; Yu, Y. M.; Seraji, S. M.; Yu, B.; Wang, H.; Song, P. A. A lava-inspired micro/nano-structured ceramifiable organic-inorganic hybrid fire-extinguishing coating. *Matter* **2022**, *5*, 911–932.

[6] Zhang, S.; Wang, R. P.; Liu, J. X.; Huo, S. Q.; Song, P. A.; Hu, X. R.; Li, B.; Xu, M. J. Ultra-efficient, organic–inorganic hybrid, highly-intumescent fire-retardant coatings for various construction materials. *Constr. Build. Mater.* **2025**, *489*, 142439.

[7] Troitzsch, J. H. Fire performance durability of flame retardants in polymers and coatings. *Adv. Ind. Eng. Polym. Res.* **2024**, *7*, 263–272.

[8] Lian, Y. C.; Wang, X. J.; Chen, S. Y.; Xiang, S. Y.; Wang, Y. C.; Tao, S. Y.; Liu, W. D. TiO_2-doped silicone nanofilament-coated fabric: A superhydrophobic platform for high-efficiency oil-water separation and self-cleaning. *ACS Appl. Polym. Mater.* **2025**, *7*, 9909–9919.

[9] Lisi, E.; Amabili, M.; Meloni, S.; Giacomello, A.; Casciola, C. M. Self-recovery superhydrophobic surfaces: Modular design. *ACS Nano* **2018**, *12*, 359–367.

[10] Liu, W. D.; Xiang, S. Y.; Liu, X. Y.; Yang, B. Underwater superoleophobic surface based on silica hierarchical cylinder arrays with a low aspect ratio. *ACS Nano* **2020**, *14*, 9166–9175.

[11] Liu, W. D.; Liu, X. Y.; Xiang, S. Y.; Chen, Y. X.; Fang, L. P.; Yang, B. Functional interface based on silicon artificial chamfer nanocylinder arrays (CNCAs) with underwater superoleophobicity and anisotropic properties. *Nano Res.* **2016**, *9*, 3141–3151.

[12] Liu, W. D.; Kappl, M.; Butt, H. J. Tuning the porosity of supraparticles. *ACS Nano* **2019**, *13*, 13949–13956.

[13] Huang, G.; Yengannagari, A. R.; Matsumori, K.; Patel, P.; Datla, A.; Trindade, K.; Amarsanaa, E.; Zhao, T. H.; Köhler, U.; Busko, D. et al. Radiative cooling and indoor light management enabled by a transparent and self-cleaning polymer-based metamaterial. *Nat. Commun.* **2024**, *15*, 3798.

[14] Khaskhoussi, A.; Rahimi, E.; Calabrese, L.; Cornet, A.; Anusuyadevi, P. R.; Gonugunta, P.; Mol, A.; Proverbio, E. Advanced durable ceramic-polymer ultra-superhydrophobic coating with anti-icing, anti-vapor condensation, and corrosion-resistant properties. *Chem. Eng. J.* **2025**, *515*, 163767.

[15] Rasitha, T. P.; Krishna, N. G.; Anandkumar, B.; Vanithakumari, S. C.; Philip, J. A comprehensive review on anticorrosive/antifouling superhydrophobic coatings: Fabrication, assessment, applications, challenges and future perspectives. *Adv. Colloid Interface Sci.* **2024**, *324*, 103090.

[16] Boinovich, L. B.; Emelyanenko, A. M. Recent progress in understanding the anti-icing behavior of materials. *Adv. Colloid Interface Sci.* **2024**, *323*, 103057.

[17] Son, S. M.; Kim, M.; Yoo, J. J.; Kim, M. S.; Kim, B. S.; Seong, D. G. Fabrication of carbon fiber/polyamide 6 composites with water resistance and anti-icing performance using a superhydrophobic fluorinated-polydopamine coating. *Compos. Sci. Technol.* **2023**, *238*, 110048.

[18] Buddingh, J. V.; Hozumi, A.; Liu, G. J. Liquid and liquid-like surfaces/coatings that readily slide fluids. *Prog. Polym. Sci.* **2021**, *123*, 101468.

[19] Rosenhek-Goldian, I.; Kampf, N.; Klein, J. Trapped aqueous films lubricate highly hydrophobic surfaces. *ACS Nano* **2018**, *12*, 10075–10083.

[20] Chen, S. P.; Li, H. Q.; Lai, X. J.; Zhang, S. F.; Zeng, X. R. Superhydrophobic and phosphorus-nitrogen flame-retardant cotton fabric. *Prog. Org. Coat.* **2021**, *159*, 106446.

[21] Bemerw Kassaun, B.; Fatehi, P. Solvent-free lignin-silsesquioxane wood coating formulation with superhydrophobic and flame-retardant functionalities. *Chem. Eng. J.* **2024**, *493*, 152582.

[22] Tsai, M. T.; Chang, S. W.; Chen, Y. J.; Chen, H. L.; Lan, P. H.; Chen, D. C.; Ko, F. H.; Lo, Y. C.; Wang, H. C.; Wan, D. H. Scalable, flame-resistant, superhydrophobic ceramic metafibers for sustainable all-day radiative cooling. *Nano Today* **2023**, *48*, 101745.

[23] Tang, Z. L.; Gao, M. H.; Li, H. D.; Zhang, Z. Y.; Su, X. Y.; Li, Y. G.; Han, Z. S.; Lv, X. M.; He, J.; Zheng, Z. H. et al. Facile and effective construction of superhydrophobic, multi-functional and durable coatings on steel structure. *Compos. Part B: Eng.* **2024**, *287*, 111850.

[24] Long, M. Y.; Peng, S.; Deng, W. S.; Miao, X. R.; Wen, N.; Zhou, Q. N.; Yang, X. J.; Deng, W. L. A robust superhydrophobic PDMS@$ZnSn(OH)_6$ coating with under-oil self-cleaning and flame retardancy. *J. Mater. Chem. A* **2017**, *5*, 22761–22771.

[25] Liu, Z. L.; Ji, T. X.; Xu, N.; Yang, C. H.; Chu, H. Q. Simple coating method for the preparation of superhydrophobic flame-retardant cotton fabrics with excellent mechanical stability performance. *Prog. Org. Coat.* **2024**, *191*, 108440.

[26] Tang, Z. L.; Gao, M. H.; Zhang, Z. Y.; Su, X. Y.; Li, Y. G.; Han, Z. S.; Lv, X. M.; He, J.; Li, H. D.; Zheng, Z. H. et al. Biomimetic construction of green, fire-proof and super-hydrophobic multifunctionality-integrated coatings via one-step spraying method for steel structures. *Colloids Surf. A: Physicochem. Eng. Asp.* **2024**, *683*, 133056.

[27] Shi, X. H.; Liu, Q. Y.; Li, X. L.; Du, A. K.; Niu, J. W.; Li, Y. M.; Li, Z.; Wang, M.; Wang, D. Y. Construction phosphorus/nitrogen-containing flame-retardant and hydrophobic coating toward cotton fabric via layer-by-layer assembly. *Polym. Degrad. Stab.* **2022**, *197*, 109839.

[28] Jiang, X. W.; Liu, S. J.; Yang, Q. Q.; Sun, D. L.; Yang, K. L.; Yuan, Z. Q.; Yu, M. G.; Meng, S. T.; Li, C. C.; Li, X. Y. et al. Facile fabrication of highly flame-retardant superhydrophobic coatings on kraft paper via a simple and efficient method. *Colloid Interface Sci. Commun.* **2023**, *57*, 100755.
[29] Zhang, D. Q.; Williams, B. L.; Shrestha, S. B.; Nasir, Z.; Becher, E. M.; Lofink, B. J.; Santos, V. H.; Patel, H.; Peng, X. H.; Sun, L. Y. Flame retardant and hydrophobic coatings on cotton fabrics via sol-gel and self-assembly techniques. *J. Colloid Interface Sci.* **2017**, *505*, 892–899.
[30] Si, Y. F.; Yang, J. Q.; Wang, D.; Shi, S.; Zhi, C. W.; Huang, K. S.; Hu, J. L. Bioinspired hierarchical multi-protective membrane for extreme environments via Co-electrospinning-electrospray strategy. *Small* **2024**, *20*, 2304705.
[31] Dogan, M.; Dogan, S. D.; Savas, L. A.; Ozcelik, G.; Tayfun, U. Flame retardant effect of boron compounds in polymeric materials. *Compos. Part B: Eng.* **2021**, *222*, 109088.
[32] Yang, J.; Jia, J. X.; Wang, X. C.; Zhao, Y. J. Bioinspired asymmetric double-layer dressings for stepwise treatment of hemorrhagic wounds. *ACS Mater. Lett.* **2024**, *6*, 1130–1139.
[33] Chen, S. S.; Li, X.; Li, Y.; Sun, J. Q. Intumescent flame-retardant and self-healing superhydrophobic coatings on cotton fabric. *ACS Nano* **2015**, *9*, 4070–4076.
[34] Dodi, G.; Popescu, D.; Cojocaru, F. D.; Aradoaei, M.; Ciobanu, R. C.; Mihai, C. T. Use of Fourier-transform infrared spectroscopy for DNA identification on recycled PET composite substrate. *Appl. Sci.* **2022**, *12*, 4371.
[35] Lin, D. M.; Zeng, X. R.; Li, H. Q.; Lai, X. J.; Wu, T. Y. One-pot fabrication of superhydrophobic and flame-retardant coatings on cotton fabrics via sol-gel reaction. *J. Colloid Interface Sci.* **2019**, *533*, 198–206.
[36] Zhu, J. Q.; Lu, X.; Yang, H. Y.; Xin, Z. Vinyl polysiloxane microencapsulated ammonium polyphosphate and its application in flame retardant polypropylene. *J. Polym. Res.* **2018**, *25*, 107.
[37] Li, X. P.; Shan, H. T.; Cao, M.; Li, B. A. Mussel-inspired modification of PTFE membranes in a miscible THF-Tris buffer mixture for oil-in-water emulsions separation. *J. Membr. Sci.* **2018**, *555*, 237–249.
[38] Liu, X.; Bai, Y. F.; Xu, J.; Xu, Q. C.; Xiao, L. P.; Sun, L. P.; Weng, J.; Zhao, Y. L. Robust amphiphobic few-layer black phosphorus nanosheet with improved stability. *Adv. Sci.* **2019**, *6*, 1901991.
[39] Amadu, M.; Pegg, M. J. Analytical derivation of a pH dependent contact angle equation and the relationship to industrial processes of energy concerns. *J. Petrol. Sci. Eng.* **2019**, *174*, 844–858.
[40] Chatelier, R. C.; Drummond, C. J.; Chan, D. Y. C.; Vasic, Z. R.; Gengenbach, T. R.; Griesser, H. J. Theory of contact angles and the free energy of formation of ionizable surfaces: Application to heptylamine radio-frequency plasma-deposited films. *Langmuir* **1995**, *11*, 4122–4128.
[41] Chen, Z. X.; Bi, X. Y.; Shi, Y. L.; Xue, D.; Li, T. Y.; Zhang, B. J.; Gao, Z. Q.; Zhao, T. Dual covalent crosslinking strategy to fabricate flame-retardant, hydrophobic, high-strength and breathable fabric. *Chem. Eng. J.* **2025**, *520*, 165781.
[42] Sai, L. M.; Ke, X. C.; Cai, Y.; Dong, S. Y.; Jia, H. X.; Cao, L.; Wu, Z.; Wang, F. F. PVDF/fluorescent carbon dots electrospun nanofibers with synergistic dipole alignment and multifunctional sensing applications. *Appl. Mater. Today* **2024**, *36*, 102025.
[43] Du, J. Y.; Fan, X. L.; Xin, F.; Chen, Y.; Feng, K. X.; Hu, J. Y. Novel coating flame retardant APP@UiO for preparation of flame retardant unsaturated polyester resin composites. *Eur. Polym. J.* **2024**, *207*, 112820.
[44] Chen, Y.; Qiu, L. L.; Ma, X. Y.; Chu, Z. D.; Zhuang, Z. S.; Dong, L. K.; Du, P. F.; Xiong, J. Electrospun PMIA and PVDF-HFP composite nanofibrous membranes with two different structures for improved lithium-ion battery separators. *Solid State Ionics* **2020**, *347*, 115253.
[45] Wang, Y. C.; Zhao, J. P. Facile preparation of slag or fly ash geopolymer composite coatings with flame resistance. *Constr. Build. Mater.* **2019**, *203*, 655–661.
[46] Yuan, B. H.; Sun, Y. R.; Chen, X. F.; Shi, Y. Q.; Dai, H. M.; He, S. Poorly-/well-dispersed graphene: Abnormal influence on flammability and fire behavior of intumescent flame retardant. *Compos. Part A: Appl. Sci. Manuf.* **2018**, *109*, 345–354.
[47] Yang, W. M.; Wu, S. Y.; Yang, W.; Chun-Yin Yuen, A.; Zhou, Y.; Yeoh, G.; Boyer, C.; Wang, C. H. Nanoparticles of polydopamine for improving mechanical and flame-retardant properties of an epoxy resin. *Compos. Part B: Eng.* **2020**, *186*, 107828.
[48] Duan, H. D.; Zhuang, C. Y.; Mei, F. C.; Zeng, C.; Pashameah, R. A.; Huang, M. N.; Alzahrani, E.; Gao, J.; Han, Y. X.; Yu, Q. et al. Benzyl(4-fluorophenyl)phenylphosphine oxide-modified epoxy resin with improved flame retardancy and dielectric properties. *Adv. Compos. Hybrid Mater.* **2022**, *5*, 776–787.
[49] Lian, R. C.; Guan, H. C.; Zhang, Y. Q.; Ou, M. Y.; Jiang, Y. P.; Liu, L.; Jiao, C. M.; Chen, X. L. A green organic-inorganic PAbz@ZIF hybrid towards efficient flame-retardant and smoke-suppressive epoxy coatings with enhanced mechanical properties. *Polym. Degrad. Stab.* **2023**, *217*, 110534.
[50] Wan, M.; Shi, C. L.; Qian, X. D.; Qin, Y. P.; Jing, J. Y.; Che, H. L.; Ren, F.; Li, J.; Yu, B.; Zhou, K. Q. Design of novel double-layer coated ammonium polyphosphate and its application in flame retardant thermoplastic polyurethanes. *Chem. Eng. J.* **2023**, *459*, 141448.
[51] Xu, Z. X.; Zhang, C. X.; He, Z. X.; Wang, Q. Pyrolysis Characteristic and kinetics of Polyvinylidene fluoride with and without Pine Sawdust. *J. Anal. Appl. Pyrolysis* **2017**, *123*, 402–408.
[52] Saboori, R.; Azin, R.; Osfouri, S.; Sabbaghi, S.; Bahramian, A. Synthesis of fluorine- doped silica-coating by fluorosilane nanofluid to ultrahydrophobic and ultraoleophobic surface. *Mater. Res. Express* **2017**, *4*, 105010.
[53] Senthil, R. A.; Theerthagiri, J.; Madhavan, J.; Arof, A. K. M. High performance dye-sensitized solar cell based on 2-mercaptobenzimidazole doped poly(vinylidinefluoride-co-hexafluoropropylene) based polymer electrolyte. *J. Macromol. Sci. Part A* **2016**, *53*, 245–251.
[54] Sha, Z.; Boyer, C.; Li, G.; Yu, Y. Y.; Allioux, F. M.; Kalantar-Zadeh, K.; Wang, C. H.; Zhang, J. Electrospun liquid metal/PVDF-HFP nanofiber membranes with exceptional triboelectric performance. *Nano Energy* **2022**, *92*, 106713.
[55] Pereira da Silva, I.; Maged, A.; Pinheiro Lima Abreu, V.; Luisa Quintanilha Candido, A.; Denise Ferreira Rocha, S.; Coutinho de Paula, E. Transfiguration of discarded PVDF ultrafiltration membranes: Optimization of pyrolysis parameters for high-value char production. *Waste Manage.* **2024**, *190*, 360–369.
[56] Maheshwaran, C.; Mishra, K.; Kanchan, D. K.; Kumar, D. Mg^{2+} conducting polymer gel electrolytes: Physical and electrochemical investigations. *Ionics* **2020**, *26*, 2969–2980.
[57] Chu, Z. L.; Olveira, S.; Seeger, S. A facile, sustainable strategy towards the preparation of silicone nanofilaments and their use as antiwetting coatings. *ChemistrySelect* **2017**, *2*, 5463–5468.